NRIAG JOURNAL OF ASTRONOMY AND GEOPHYSICS
2020, VOL. 9, NO. 1, 245–259
https://doi.org/10.1080/20909977.2020.1723867

Investigating groundwater corrosion and overburden protective capacity in a low latitude crystalline basement complex of southwestern Nigeria

M. A. Adabanija and R. A. Ajibade

Department of Earth Sciences, Ladoke Akintola University of Technology, Ogbomoso, Nigeria

ABSTRACT

The total longitudinal conductance S obtained from the interpretations of vertical electrical soundings data acquired near 40 well bores was calibrated using total dissolved solids (measured in situ) in the sampled wells' groundwater to determine the overburden protective capacity and groundwater corrosion in a crystalline basement complex of Ogbomoso North, southwestern Nigeria. The acidity (pH) and electrical conductivity (EC) were also measured. Groundwater corrosiveness was determined using the Langelier saturation index (LSI) and the aggressive index (AI). The computed S of predominantly H-, KH-, QH-, HA- and HKH- types resistivity curve was 0.037995– 1.10878 mhos. The TDS, pH and EC of the water samples measured 36–747 ppm, 6.15–9.3 and 74–1491 µS/cm, respectively. The regression equation of the TDS-based S calibration curve indicates a strong positive correlation (R2 = 0.8932) and revealed the overburden protective capacity ranged from excellent to good, fair and poor. The computed LSI and AI were −3.61 to 1.2 and 7.8–12.8, respectively. The high values of both LSI (0.2–1.2) and AI (11.2–12.8) in the southwestern part suggest groundwater there is strongly corrosive, while low values of −3.6 to −1.2 and 7.8–10.2 in the northwestern and southeastern parts indicate non-corrosive groundwater.

ARTICLE HISTORY
Received 16 August 2019
Revised 14 January 2020
Accepted 27 January 2020

KEYWORDS
Groundwater corrosion; overburden protective capacity; corrosive index; total dissolved solids; vertical electrical sounding

1. Introduction

Groundwater is the most important source for domestic, industrial and agricultural water supply in the world, and is regarded as having more mineral contents compared to surface water (Mirribasi et al. 2008). The chemical composition of groundwater has been attributed to a combination of the composition of water entering the groundwater reservoir and reactions with minerals present in the rocks (Zhu et al. 2008; Iliopoulus et al. 2011). Groundwater vulnerability assessment is therefore vital for groundwater resources management and land-use planning (Rupert 2001; Babiker et al. 2005; Machiwal et al. 2018). However, while several efforts have been and are being made to characterise the groundwater facies in an effort to ascertain and assess groundwater quality (e.g. Adabanija et al. 2015; Olasehinde 2015; Machiwal et al. 2018), little attention has been given to assessments of the vulnerability/susceptibility of geologic material as a medium to the contaminants that result from pollution of the groundwater (e.g. Rupert 2001; Babiker et al. 2005; Akinwumiju and Olorunfemi 2017; Zuquette and Failache 2018). Furthermore, one of the most common problems affecting domestic water supplies is corrosion, a chemical process that slowly dissolves metal, resulting in deterioration and failure of plumbing pipes, fixtures and water-using equipment (Figures 1 and 2). Water with a low pH (i.e. a high level of acidity) increases the rate of corrosion due to the presence of hydrogen ions. Untreated corrosive water can dissolve lead, especially in the absence of protective scale, metallic pipes and other components of water distribution systems (Edwards and Triantafyllidou 2007; Hu et al. 2012; Pieper et al. 2015; Belitz et al. 2016). The degree of acidity (pH) and alkalinity (calcium, carbon dioxide, chloride, sulphate and oxygen), total dissolved solids (TDS) and temperature are the most important factors determining corrosion. Though the earth's medium acts as a natural filter to percolating fluid (Barker et al. 2001), the use of chemical products and indiscriminate waste disposal are potential sources of groundwater contamination (Obiora et al. 2015). The degree of contamination has been linked to the permeability, porosity and thickness of the geologic materials overlying the aquifer (Obiora et al. 2015). For instance, while unconsolidated and non-compacted geologic material such as coarse sand is capable of enhancing the percolation of effluents into the subsurface to contaminate groundwater (Keswick et al. 1982), clay/clayey soils of low resistivity and hence low hydraulic conductivity are inhibitors of contaminants (De Oliveira Braga et al. 2006). The electrical properties of the geologic material overlying the aquifer are therefore important and can be determined using either invasive techniques, involving electrical borehole logging, or non-invasive

CONTACT M. A. Adabanija maadabanija@lautech.edu.ng Department of Earth Sciences, Ladoke Akintola University of Technology, Ogbomoso, Nigeria

Figure 1. Effect of corrosion on metallic material: (a) replacement of metallic pipes by PVC after leakage and clogging problems; (b) corrosion problem on metallic pipe joints; (c) pinhole leaks in copper tubing caused by internal corrosion (adapted from McFarland et al. 2011).

Figure 2. Effect of metallic corrosion: (a) gate valve out of order; (b) thread of pipe damaged; (c) gate valve starting to scale and rusting; and (d) metallic material, pipe, almost changed into soil due to corrosion (Source: Corrosionpedia.com).

methods, such as vertical electrical sounding (VES; e.g. Hodlur et al. 2010). Exploratory drilling and geophysical well logging are equally practical solutions for exploration programmes (e.g. Kwang et al. 2004) but can be expensive (Hodlur et al. 2010). Conversely, the VES technique is simple and inexpensive (Dhakate and Singh 2005), with ability to image structures at scales from millimetres to kilometres (Storz et al. 2000; Linderholm et al. 2008). VES is capable of detecting changes in the electrical conductivity of the subsurface layers that reflect the fluid content of such layers (Hwang et al. 2004) and is useful for hydrostratigraphic sequencing and analysis (e.g. Ismail et al. 2005; Clifford and Binley 2010; Mastrocicco et al. 2010). Specifically, Schlumberger VES arrays are designed to discriminate electrical resistivity associated with lithologic versus hydrologic characteristics (Zohdy et al. 1974; Hodlur et al. 2006). VES data are interpreted in terms of resistivity and thickness – layering parameters – of a geoelectric layer. The secondary parameters, also known as geoelectric parameters, are derived from the layering parameters (Zohdy et al. 1974). These include the Dar Zarrouk parameters: total longitudinal conductance and total transverse resistance (Maillet 1947), average longitudinal resistivity, average transverse resistivity and anisotropy. The parameters are derived considering a column of unit square cross-section area out of a group of layers (Zohdy et al. 1974; Khalil 2006).

Longitudinal conductance has been used to assess the protective capacity of the overburden units (e.g. Henriet 1976; Oladapo et al. 2004; Obiora et al. 2015; Bayewu et al. 2018). However, rather than calibrating

the longitudinal conductance using either in situ or laboratory measured parameter(s), it is usually measured in absolute terms without determining the infiltration time (e.g. Henriet 1976) or vertical times-of-travel (e.g. Kalinski et al. 1993) through unsaturated groundwater protective layers and compared with values obtained by Henriet (1976), especially in sub-Sahara Africa (e.g. Oladapo et al. 2004; Ayolabi 2005, Oladapo and Akintorinwa 2007; Atakpo and Ayolabi 2009, Obiora et al. 2015; Bayewu et al. 2018) the contributions of the anthropogenic sources or local geology were not also considered. In the current study, the overburden protective capacity, computed as total longitudinal conductance of the overburden material using geoelectrical layering parameters obtained from iterative interpretation of VES data acquired near well bores in Ogbomoso North, southwestern Nigeria, has been calibrated. This was accomplished by employing in situ physical parameters, specifically TDS, for the assessment of the protective capacity of the aquifer attributed to the capability of TDS to account for both geogenic and anthropogenic effects on groundwater as well as its capability as a good indicator of groundwater mineralisation. High TDS also enhances the conductivity of current by water, which promotes metallic corrosion (Singley et al. 1985, p. 16). The specific objectives include qualitative and quantitative determination of the sensitivity of groundwater to pollution and corrosiveness. The aquifers in the area were previously established as localised and lying within the weathered and fractured basement (Adabanija et al. 2015).

2. Location, and geological and hydrogeological setting

The study area is located in Ogbomoso North, southwestern Nigeria, within longitudes 004°13′42″ E–004°17′18″E and latitudes 008°06′52″–008°12′48″N Figure 3. The topography is relatively rugged, with elevation varying between 330 and 390 m and averaging about 360 m above sea level. The drainage pattern is dendritic (Figure 3). Stream and river flow is considerably reduced in the dry season and sustained by effluent seepage. In the raining season, the rivers are turbid as a result of high clay content from the upper reaches, while the smaller streams become local puddles with small connecting trickles. The study area exhibits the typical tropical climate of average high temperatures, high relative humidity and generally two rainfall maxima regimes during the rainfall period of March to October. The mean temperatures are highest at the end of the Harmattan (averaging 28°C) – that is, from the middle of January to the onset of the rains in the middle of March.

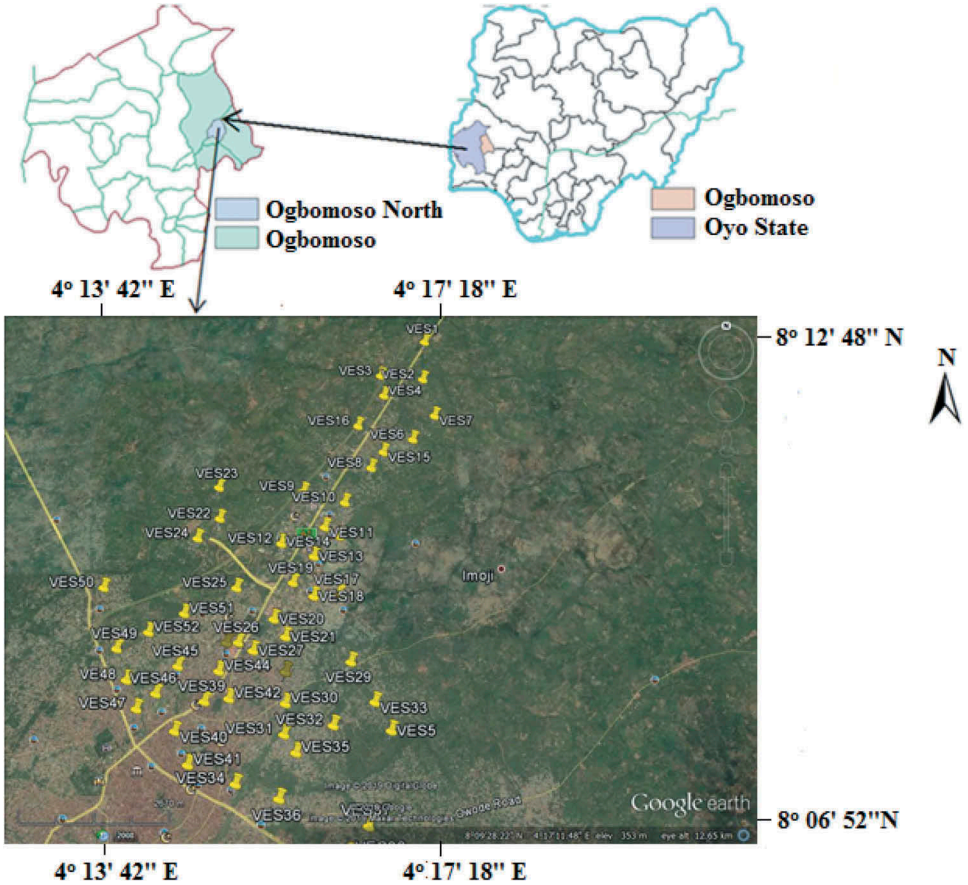

Figure 3. Vertical electrical sounding (VES) and groundwater sampling points.

Ogbomoso falls within the Precambrian basement complex of southwestern Nigeria, which comprises migmatite-gneiss, banded-gneiss, porphyroblastic biotite-gneiss, granite and quartzite (Rahaman 1976).

The quartzites occur as elongated ridges trending NW–SE and are mostly massive. Schistose quartzites with micaceous minerals alternating with quartzo-feldsparthic ones are common in the southern part (Figure 4). The gneisses are the dominant rock type, occurring as granite gneisses and banded gneisses with coarse to medium-grained texture. Noticeable minerals include quartz, feldspar and biotite. Structural features exhibited by these rocks are foliation, faults, joints and microfolds which have implications for groundwater accumulation and movement.

Hydrogeologically, the fractured/weathered basement constitutes the aquifer units (confined/unconfined) within the area, while the conductive zones comprise clay and sandy clay/clayey sand. Both the basement relief map and the basement resistivity map display a horst model with correspondence between depressions and low-resistivity zones (fracture basement) at the western part of the study area, which could be regarded as a groundwater discharge or collection zone. The groundwater recharge zone is located in the north and northeast (Adabanija et al. 2015).

3. Material and method

3.1. Determination of physico-chemical parameters

The detailed field investigation was preceded by a reconnaissance survey involving an inventory of wells. Forty wells (Figure 1) of depth 8–45 m were eventually selected, from which groundwater samples were collected. Physical parameters – namely, electrical conductivity (EC), pH, temperature and TDS – were measured in situ using a pre-calibrated portable handheld HI98130 meter.

3.2. Groundwater corrosion indices

The corrosiveness of water can be estimated by the calculation of one or more corrosion indices. A corrosion index is a mathematical formulation based on the

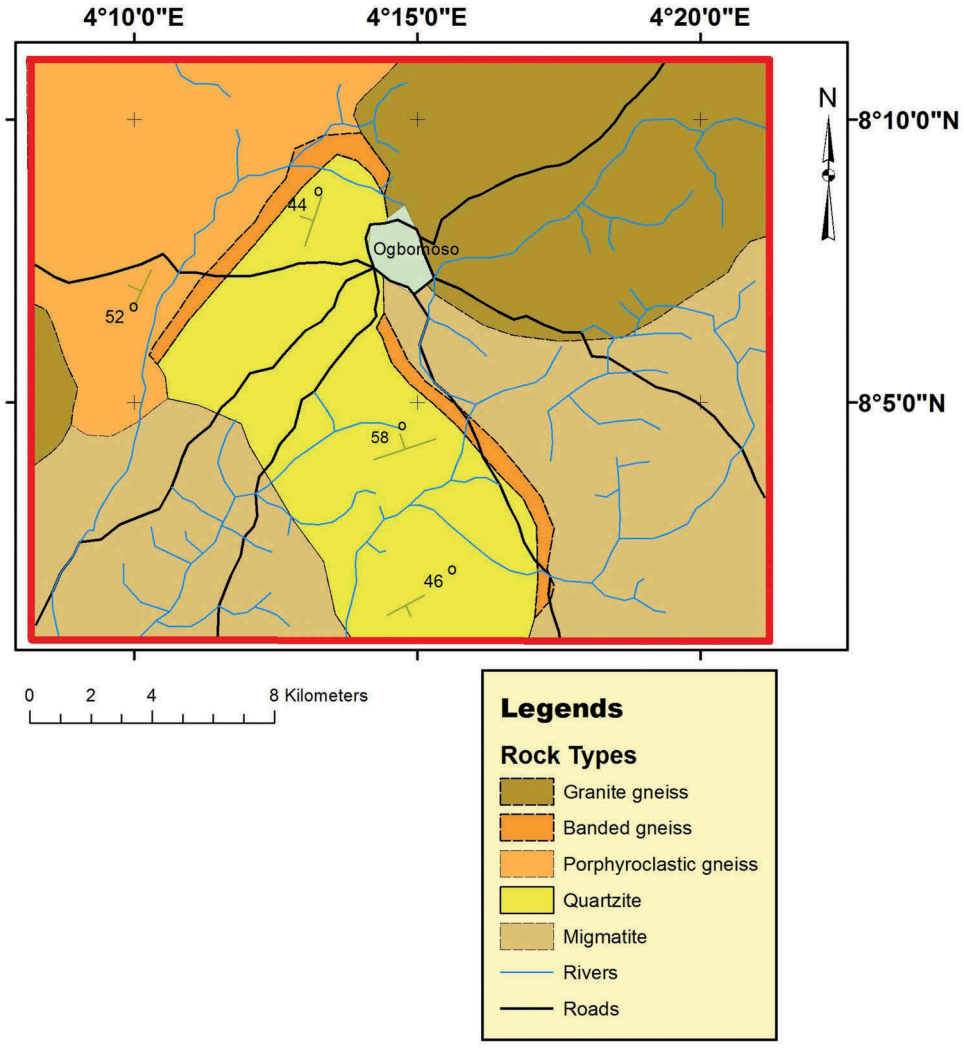

Figure 4. Geologic map of Ogbomoso (after Afolabi et al. 2013).

concentrations of various chemical constituents and the physical properties of the water. The corrosion indices used are empirical formulations derived from experimental work and comprise the following.

3.2.1. Langelier saturation index

The Langelier saturation index (LSI) is an equilibrium model derived from the theoretical concept of saturation and provides an indicator of the degree of saturation of water with respect to calcium carbonate (Langelier 1936). The Langelier saturation level approaches the concept of saturation using pH as a main variable. Thus, the LSI can be interpreted as the pH change required for water to reach equilibrium. Water with an LSI of 1.0 is 1 pH unit above saturation. Reducing the pH by 1 unit will bring the water into equilibrium. This occurs because the portion of total alkalinity present as CO_3^{2-} decreases as the pH decreases, according to the equilibrium describing the dissociation of carbonic acid.

The algebraic difference between the actual pH of a sample of water and its computed pHs is called the calcium carbonate saturation index. Hence, the saturation index equals pH minus pHs.

$$\text{Langelier Saturation Index (LSI)} = \text{pH} - \text{pHs} \quad (1)$$

where

$$\text{pHs} = \text{A} + \text{B} - \log\left(\text{Ca}^{2+}\right) - \log(\text{total alkalinity}) \quad (2)$$

Ca^{2+} and total alkalinity are expressed as mg/L of equivalent calcium carbonate. For the calculation of pHs, factor A was calculated at any temperature using the following equation:

$$\text{A} = 2.24961 - .017853\ \text{T} + .00008238\ \text{T}^2 - .00000041\ \text{T}^3 \quad (3)$$

Factor B was calculated using the following equation, from Larson and Buswell (1942):

$$\text{B} = 9.7 + \frac{2.5\sqrt{\mu}}{1.0 + 5.3\sqrt{\mu} + 5.5\mu} \quad (4)$$

$$\mu = (0.000025 \text{ x TDS}) \quad (5)$$

The LSI indicates whether water is supersaturated or undersaturated with respect to calcium carbonate, and thus whether or not a protective film of calcium carbonate can be precipitated on pipe interiors. Negative LSI values indicate undersaturation with respect to calcium carbonate, indicating calcium carbonate scale is not likely to form; otherwise, the water is supersaturated and calcium carbonate precipitation is favoured (Langelier 1936). LSI values close to zero are considered borderline (Roberge 2007).

3.2.2. Aggressive index

The aggressive index (AI) is essentially a simplified version of the LSI, and is given by the equation:

$$\text{AI} = \text{pH} + \log\,[\text{AH}] \quad (6)$$

where A is alkalinity and H is calcium hardness (or concentration of calcium expressed as mg/L of equivalent $CaCO_3$; American Water Works Association 1977).

AI values of 12.0 or greater indicate non-aggressive (non-corrosive) water. Values from 10.0 to 11.9 indicate that the water is moderately aggressive, whereas values of less than 10.0 indicate the water is highly aggressive. Like the LSI, the AI indicates the degree of saturation with respect to calcium carbonate, but a value of 12.0 indicates saturation for the AI; this corresponds to an ionic strength of approximately 0.01 and a temperature of approximately 14°C (Schock and Buelow 1981, p. 636). A value of 12.0 for the AI approximates a value of zero for the LSI.

The AI was used in the United States in a nationwide survey of the corrosiveness of drinking-water supplies and generally was found to estimate adequately the aggressiveness of the waters tested (Millette et al. 1980). Although the AI is a less rigorous expression than the LSI, the AI has been used extensively and is useful as an indicator of water quality where the data needed to calculate the LSI are not available.

3.3. Electrical resistivity surveying

An electrical resistivity survey procedure employing VES was conducted using Schlumberger electrode configuration within 1.0–3.0 m around the existing 40 hand dug/deep wells (Figure 3) in the study area. The half current electrode (AB/2) spacing ranged within 1.0 to 75.0 m while the potential electrode (MN/2) was varied between 0.25 and 6.0 m. The resistance R measured as a result of the passage of current I at each sampled point was inserted into the following equation:

$$\rho_a = \text{KR} \quad (7)$$

to obtain apparent resistivity ρ_a (K is the geometric factor). The VES data are presented as apparent resistivity curves, field curves, or depth sounding or profile by plotting ρ_a against AB/2 on a bi-logarithm sheet. The apparent resistivity curves were then interpreted using a manual partial curve-matching technique to obtain the initial layering parameters, which were subsequently subjected to computer iterative interpretation using Winresist software.

3.4. Determination of aquifer vulnerability

The aquifer vulnerability was determined by considering the Dar Zarrouk parameters (Henriet 1976),

namely transverse resistance (T) and longitudinal conductance (S), explicitly defined by Equations (8) and (9), respectively, for a unit horizontal layer of a simple stratified model:

$$T = h\rho = h/\sigma \quad (8)$$

and

$$S = h/\rho = h\sigma \quad (9)$$

where h is the thickness of the saturated layer measured in metres and ρ is the electrical resistivity of the layer in ohm-metres.

This is because the combination of thickness and resistivity, as expressed by Dar Zarrouk parameters, can be used as a base for the evaluation of properties such as aquifer transmissivity and protection of groundwater resources (Henriet 1976; De Oliveira Braga et al. 2006; Golam et al. 2016). In some other applications, Dar Zarrouk parameters have been used to illustrate non-uniqueness problems associated with the interpretation of VES, employing T and S to explain equivalence for K-type apparent resistivity curve ($\rho_1 < \rho_2 > \rho_3$) and H-type apparent resistivity curve ($\rho_1 > \rho_2 < \rho_3$) geoelectrical models, respectively (Adabanija 2009). However, based on low resistivities of the clay layer the protective capacity of the overburden could be considered as proportional to the ratio of thickness to resistivity, the longitudinal conductance S (De Oliveira Braga et al. 2006). In this study, the water table can be represented on a sounding curve as a conductive or low-resistivity layer (Deppermann and Homilius 1965) overlain or underlain by a relatively high-resistivity layer(s) (Figure 5), thereby describing an H-type curve. The longitudinal conductance S was calculated for all H-type and its admixture to determine the protective capacity of the overburden overlying the aquifer. The computed S was then subsequently calibrated using the results from the analysis of water samples (specifically, TDS) to assess the protective capacity of the aquifer. This is attributed to the fact that the TDS could account for both geogenic and anthropogenic effects on groundwater and was also measured in situ.

4. Results and discussion

4.1. Electrical soundings

The sounding curves in the study area are grouped on the basis of the resistivity relationship between the layers constituting the apparentresistivity section. These include H, HA- ($\rho_1 > \rho_2 < \rho_3 < \rho_4$), HKH- ($\rho_1 > \rho_2 < \rho_3 > \rho_4 < \rho_5$), KH- ($\rho_1 < \rho_2 > \rho_3 < \rho_4$) and QH- ($\rho_1 > \rho_2 > \rho_3 < \rho_4$) apparent resistivity curve types, indicating the association between conductive or low-resistivity layers of a sounding curve overlain/underlain by a more resistive layer and the water table (Deppermann and Homilius 1965; Adabanija et al. 2008). The percentage distributions (Figure 6) indicated the curve types were in the order H type > KH type > QH type > HA type > HKH type. The interpretation indicated the H-type apparent resistivity curve (Figure 7(a)) is made up of three layers, comprising 0.8–1.8 m thick topsoil with a resistivity ranging between 50 and 3152 Ω.m, an intermediate conductive layer of resistivity 11–135 Ω.m and 2.3–13.0 m thick, and a third layer with resistivity ranging from 95 to 6207 Ω.m (Table 1). The KH type (Figure 7(b)), QH type (Figure 7(c)) and HA type (Figure 7(d)) are four-layer models of apparent resistivity curves. The summary of the interpretation of the layering parameters (Table 1) indicated the thickness of the topsoil was 0.5–1.4 m, 0.9–1.3 m and 0.6–1.6 m with corresponding resistivity of 34–879 Ω.m, 75–1138 Ω.m and 25–804 Ω.m for KH type, QH type and HA type, respectively. While the second layer is conductive and has a resistivity of 30–839 Ω.m and 17–171 Ωm with corresponding thickness of 1.1–4.5 m and 1.6–6.9 m for QH type and HA type, respectively, the 0.8–6.5 m thick second layer of KH type is

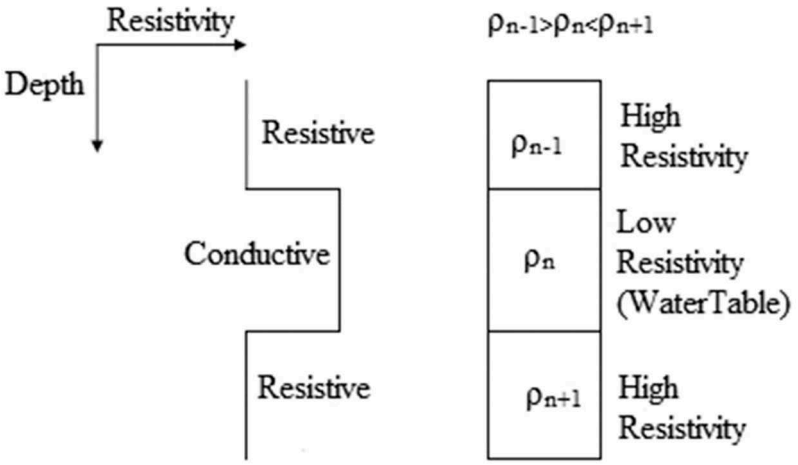

Figure 5. A conceptual geometry of water-bearing formation and overlying/underlying layers in the basement complex using a geoelectrical section (after Adabanija et al. 2008).

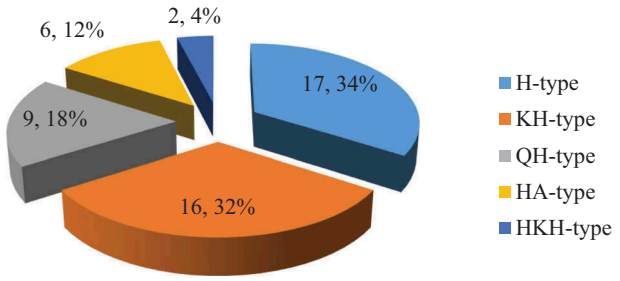

Figure 6. Pie chart representation of categories of apparent resistivity curves obtained from the study area.

relatively resistive, at 80–1224 Ω.m. However, the third layer is relatively conductive and has a resistivity of 37–105 Ω.m, 14–112 Ω.m and 50–283 Ω.m for KH type, QH type and HA type, respectively, with corresponding resistivity of the fourth layer of 110–3267 Ω.m, 74–926 Ω.m and 577–2975 Ω.m.

The HKH type depicts a five-layer model (Figure 7(e)) with resistivity of first, second, third, fourth and fifth layers of 179–199 Ω.m, 87–128 Ω.m, 231–323 Ω.m, 55–103 Ω.m and 191–525 Ω.m, respectively (Table 1). It has the thickest overburden, ranging from 43.7 to 46.7 m.

4.2. Lithology logs

The lithology logs of some of the borings based on drill cuttings (Oladunjoye et al. 2013) and the geoelectric signatures of the corresponding VES values obtained in the current study are shown in Figure 8.

The lithology log of a boring around a geoelectrically characterised H-type section (Figure 8(a)) indicates reddish lateritic clay within 0–3 m depth underlain by clayey sand with clay and sand in respective proportions of 40% and 60%, at 3.1–6.1 m depth. Brownish/reddish-stained quartz (about 50%) obtained thereafter indicates a weathered zone from 6.1 m through 12 m depth. The proportions of lateritic pan and feldspar were 40% and 10%, respectively, in this interval. However, the cuttings decreased in size while the proportion of feldspar initially increased through 12 m to 16 m

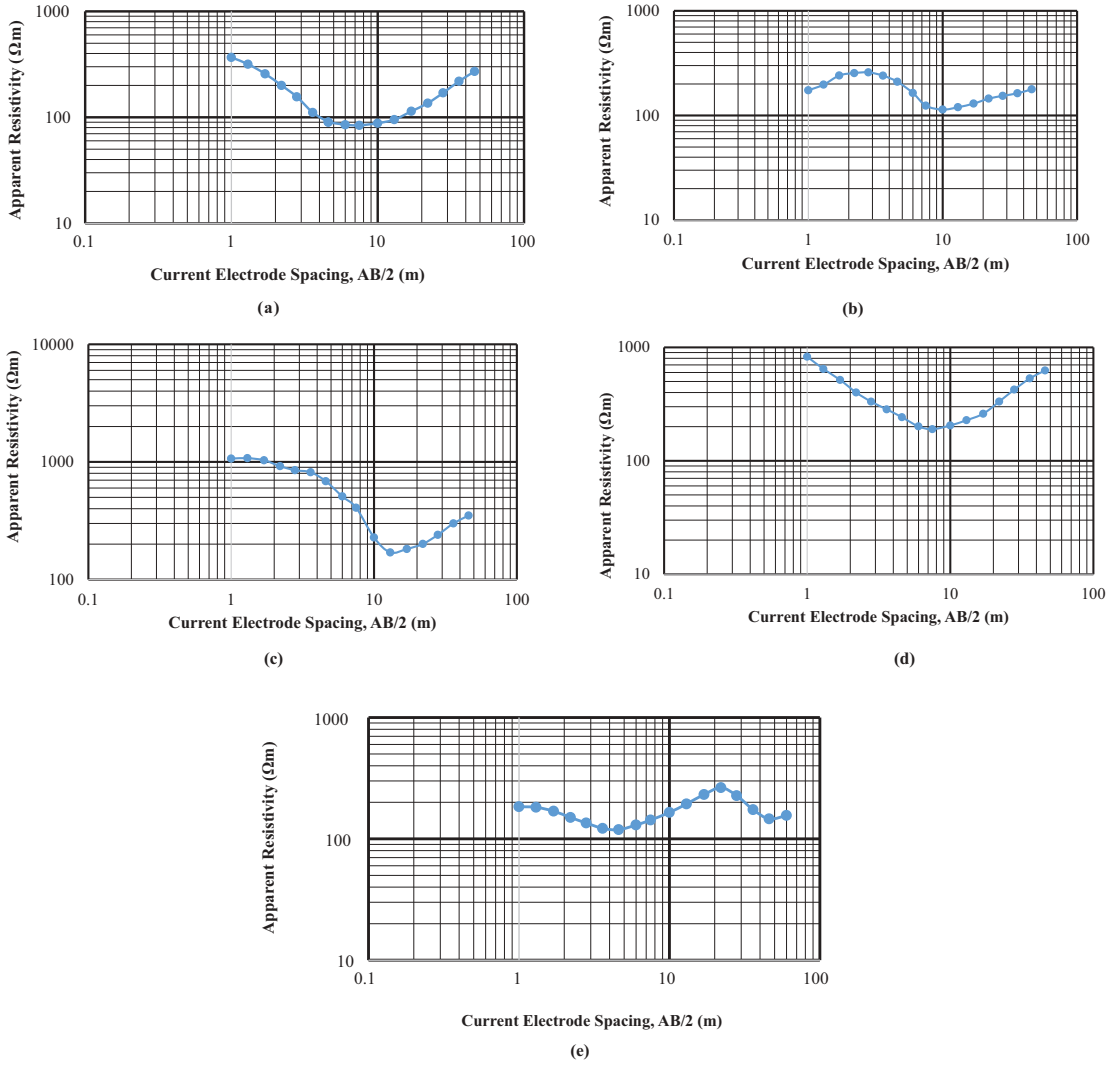

Figure 7. Showing samples of apparent resistivity curves in the study area: (a) H type; (b) KH type; (c) QH type; (d) HA type; and (e) HKH type.

Table 1. Summary of layering parameters and apparent resistivity curve types obtained from the interpretation of vertical electrical sounding (VES) data acquired near wells and bore holes in Ogbomoso North, southwestern Nigeria.

Layer	Resistivity (Ω. m)	Thickness (m)	Curve type	Depth to interface (m)
1	50–3152	0.8–1.8	H	-
2	11–135	2.3–13.0		0.8–1.8
3	95–6207	-		3.1–14.8
1	34–879	0.5–1.4	KH	-
2	80–1224	0.8–6.5		0.5–1.4
3	37–105	3.3–18.1		1.3–7.9
4	110–3267	-		4.6–26.0
1	75–1138	0.9–1.3	QH	-
2	30–839	1.1–4.5		0.9–1.3
3	14–112	4.3–30.2		2.0–5.8
4	74–926	-		6.3–36.0
1	25–804	0.6–1.6	HA	-
2	17–171	1.6–6.9		0.6–1.6
3	50–283	9.9–19.4		2.2–8.5
4	577–2975	-		12.1–27.9
1	179–199	1.1	HKH	-
2	87–128	2.7		1.1
3	231–323	17.3–17.8		3.8
4	55–103	22.6–25.1		21.1–21.6
5	191–525	-		43.7–46.7

and subsequently decreased at 18.2 m depth, where the boring was terminated.

The lithology logs obtained from one of the wells, with geoelectrical characteristics indicating an HKH-type section (Figure 8(b)), comprise lateritic pan/indurated lateritic fragments at 0–1 m depth underlain by lateritic pan held in place by clay at 1–3 m depth. The clay contents are probably responsible for the lower resistivity compared with the relatively higher resistivity of the first layer. This was, however, truncated by highly weathered material of different grain sizes comprising quartz, feldspar and biotite at 3–6 m depth, also of low resistivity. The succeeding relatively higher resistivity layer is as exemplified by fresh cuttings material with an order of abundance of mafic minerals > feldspar > quartz, suggesting gneiss at 6–9 m depth. Fines grains of biotite and quartz were subsequently obtained, indicating a weathered layer at 9–18 m depth. However, cuttings of larger sizes, consisting of equal proportions of quartz and biotite with a certain proportion of feldspar, were obtained at 18–26 m depth.

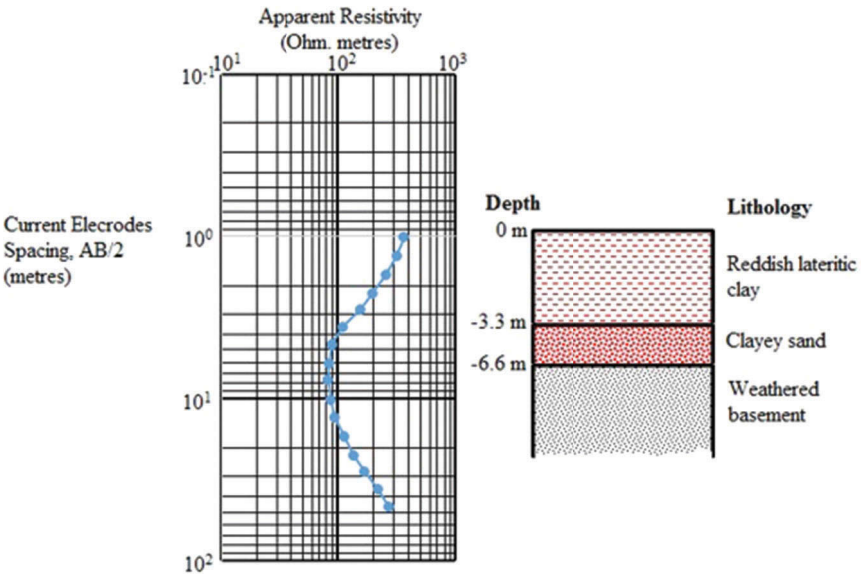

(a)

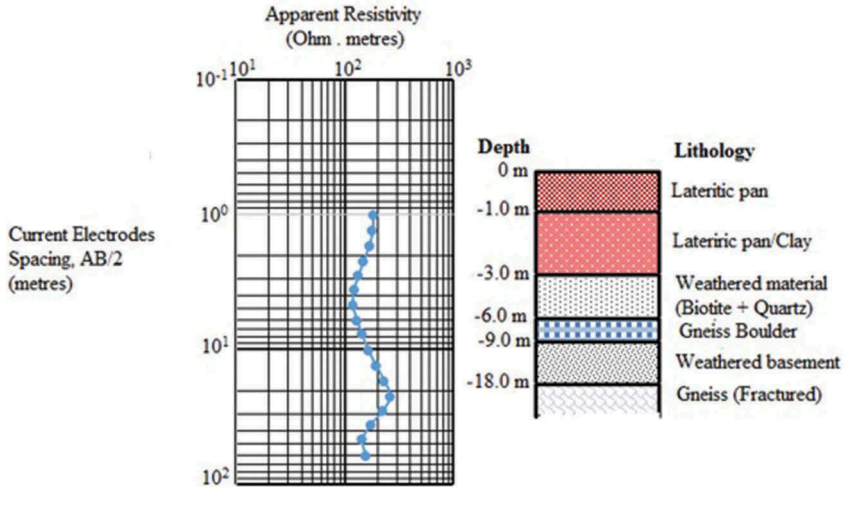

(b)

Figure 8. One-dimensional resistivity models and lithology logs of some sampled wells: (a) H-type model geoelectric section; (b) HKH-type model geoelectric section.

Large cuttings but with felsic mineral banding in approximately equal proportions were obtained at 26–35 m. This indicates fractured gneiss at 18–35 m depth.

4.3. Groundwater samples: physical parameters

The results of some physico-chemical parameters of groundwater samples collected from well bores in the study area are shown in Table 2, while the spatial distributions are illustrated in Figure 9.

Table 2. Summary of physical parameters/corrosive index of groundwater and longitudinal conductance, Ogbomoso North, southwestern Nigeria.

Parameter (n = 40)	Minimum	Maximum	Mean	WHO	Maximum
EC (µS/cm)	74	1491	90.67	1000	-
TDS (ppm)	36	747	145	500	1500
pH	6.15	9.3	7.6	7.0–8.5	9.5
AI	7.8	12.8	9.98	-	-
LSI	−3.61	1.20	−1.61	-	-
S (mho)	0.037995	1.10878	0.27009	-	-

4.3.1. Electrical conductivity

The EC values are 74–1491 µS/cm (Table 2) with an average value 90.67 µS/cm. The EC as recommended by the World Health Organization (WHO 2011) standard in domestic water is 1000 µS/cm. Thus, the EC value around the southwestern part, Isale Afon and Saja area (Figure 9(a)), is above the WHO standard and hence not good for drinking purposes, while the water in all other parts is good for domestic purposes.

4.3.2. Total dissolved solids

The TDS values range from 36 to 747 ppm (Table 2) and averaged 145 ppm in the study area. The TDS values for the groundwater around the southwestern (Isale Afon and Saja) area (Figure 9(b)) are above the WHO (2011) standard and it is therefore not good for drinking purposes, while groundwater in the remaining parts is good for domestic purposes. This is corroborated by the results obtained by ranking TDS of the groundwater in the area (Figure 10(a)) into four quartiles according to increasing TDS and the WHO

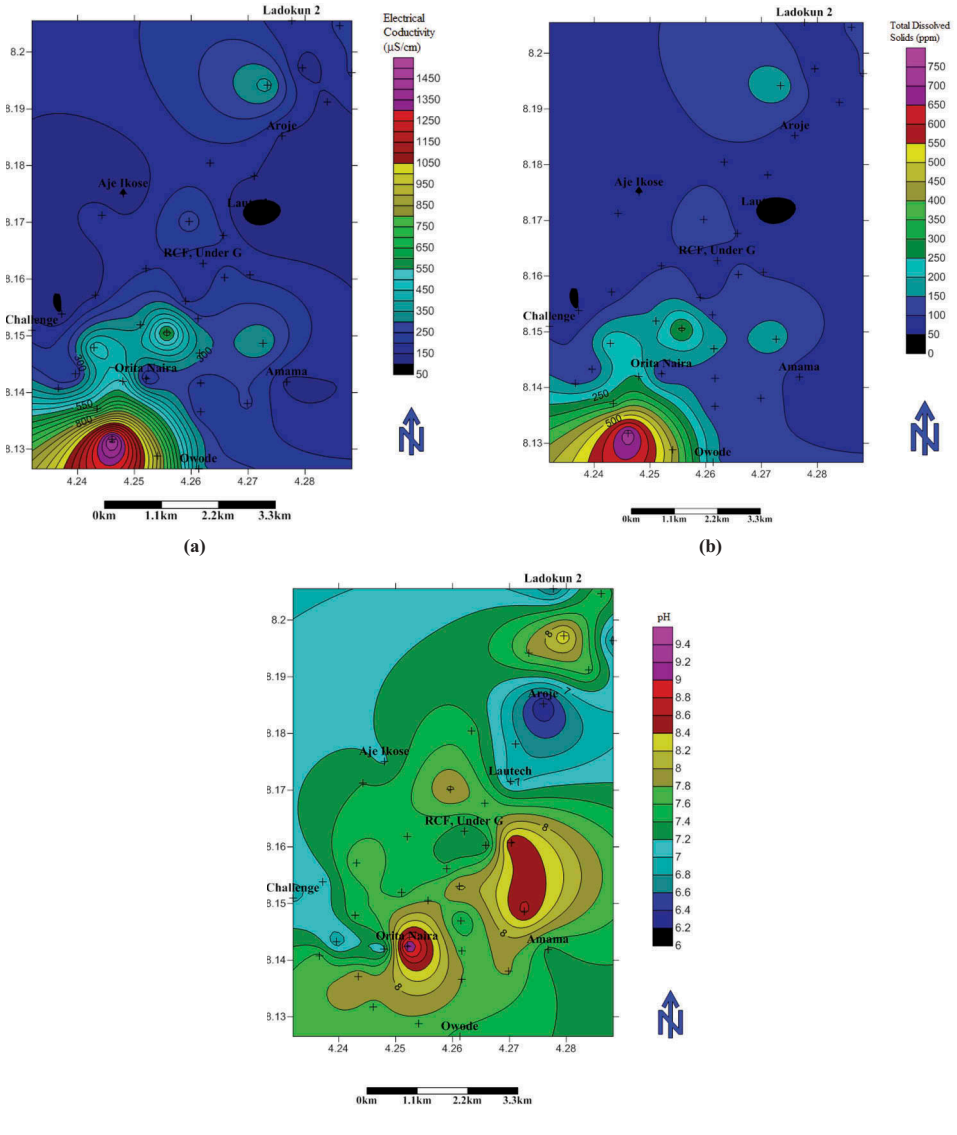

Figure 9. Spatial distribution of physical parameters of groundwater in Ogbomoso North, southwestern Nigeria: (a) electrical conductivity; (b) total dissolved solids; (c) pH.

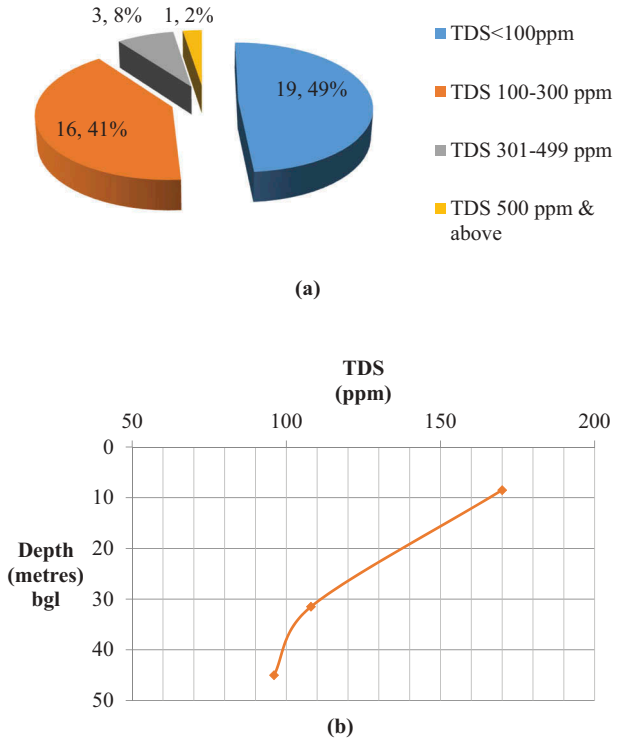

Figure 10. (a) Ranking based on WHO (2011); and (b) changes in TDS values with depth in the study area.

(2011) acceptable level, indicating just 2% of the samples had TDS groundwater contents exceeding 500 ppm. However, 49% of the samples contained TDS of less than 100 ppm with pH ranging between 6.15 and 9.30 – that is, greater than 5.5, and at depths of about 45 m and deeper (Figure 10(b)) suggest the influence of water–rock interaction on the TDS level (Rasolofonirina et al. 2004). In contrast, the TDS content of groundwater at depths of less than 10 m was the highest, with a median value of 170 ppm (Figure 10(b)), suggesting the influence of anthropogenic effects and thereby justifying the use of TDS for calibration of total longitudinal conductance. These indicate the TDS decreases with depth (Figure 10(b)), suggesting a depth of 35 m as the interface between shallow and deep groundwater or between fractured/fresh basements in the area, as corroborated by fractured gneiss at 18–35 m depth (Figure 8(b)). Furthermore, high EC as well as high TDS at Isale Afon and Saja suggest a relationship between EC and TDS as exemplified by Figure 11. The regression analysis of the plots indicates a linear relationship described by the following equation:

$$y = 1.998x + 0.9716 \quad (10)$$

where x and y are TDS and electrical conductivity, respectively, with a correlation coefficient (R^2) of 1, suggesting a strong correlation between EC and TDS. Comparing the equation with that of a straight line, as follows:

$$y = mx + c \quad (11)$$

indicates the intercept c = 0.9716, while the gradient m has a value of +1.998, revealing a direct relationship between EC and TDS – that is, the higher (lower) the EC, the higher (lower) the TDS. Thus, knowledge of either EC or TDS could be used to estimate the other, particularly in any location within the study area where measurements were not made.

4.3.3. Acidity (pH)

The acidity of the groundwater samples in the study area ranged between 6.15 and 9.3 (Table 2) with a mean of 7.6. Based on the permissible limit of 7.0–8.5 recommended for drinking purposes (WHO 2011), the groundwater in the northwest–west (Ajeikose, Challenge, Federal area), and the northeast (Abaa area) (Figure 9(c)) is considered acidic (pH < 7.0), and is capable of causing health problems such as acidosis. However, the pH values of the groundwater in the eastern and southern parts are above the WHO (2011) standard, suggesting a high sodium bicarbonate content.

4.4. Groundwater corrosion

The groundwater corrosion based on the LSI and AI is presented in Table 2. The LSI varied from −3.61 to 1.20 with an average of −1.61 for all the samples analysed, while AI ranged between 7.80 and 12.8 with a mean of 9.98. Based on the LSI interpretation of the New Jersey Department of Environmental Protection (1985) (Table 3), the groundwater in the northwestern and

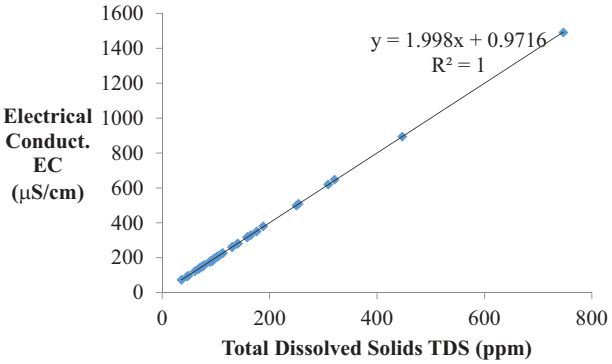

Figure 11. Plot of EC against TDS.

Table 3. Interpretation of the LSI (adapted from Langland and Dugas 1996).

Langelier	Tendency of water
LSI < −2	Intolerable corrosion
−2.0 < LSI < −0.5	Serious corrosion
−0.5 < LSI < 0	Seriously corrosive but non-scale-forming
LSI = 0	Balanced but pitting
0 < LSI < 0.5	Slightly scale-forming and corrosive
0.5 < LSI < 2	Scale-forming but non-corrosive

southeastern parts of the study area (Figure 12(a)) is non-corrosive, with LSI ranging between −3.6 and −1.2, while the high LSI values for the groundwater in the southwestern part, 0.2–1.2, indicate it is corrosive. However, according to Singley et al. (1985), AI values from 10.0 to 11.9 indicate that the water is moderately aggressive, and for values less than 10.0, the water is considered to be highly aggressive. Based thereon, the groundwater in the northwestern and southeastern parts, with AI values of 7.8–10.2 (Figure 12(b)), is non-corrosive, but the groundwater in the southwestern part with AI values of 11.2–12.8 is strongly corrosive. This suggests similar results from the LSI and AI assessments of corrosiveness of groundwater, corroborating the interpretation of AI as a simplification of the LSI.

4.5. Total longitudinal conductance

The total longitudinal conductance ranged between 0.037995 and 1.10878 mhos with a mean value of 0.27009 mhos (Table 2). The spatial distribution (Figure 13) indicated the total longitudinal conductance is low, ranging from 0.05 to 0.35 mho, in the northwestern and southeastern parts of the study area; high in the southwestern part, ranging from 0.4 to 0.7 mho; and highest at Aroje, where it is greater than 0.75 mho.

4.6. Calibration of total longitudinal conductance

The results from the calibration of total longitudinal conductance S by TDS is illustrated by the plot of median TDS values (ranked into four subsets or quartiles according to increasing TDS and the corresponding median values of S; Figure 14). They indicate a strong positive correlation, with an R^2 value of 0.8932, between TDS and S, as exemplified by the regression equation:

$$TDS = 651.84S - 0.0895 \quad (12)$$

This is corroborated by the spatial distribution maps in Figures 9(b) and 13, showing that areas of high total longitudinal conductance, specifically in the southwest, also have high TDS. Such areas also have high EC (Figure 9(a)), high LSI (Figure 12(a)) and high AI (Figure 12(b)).

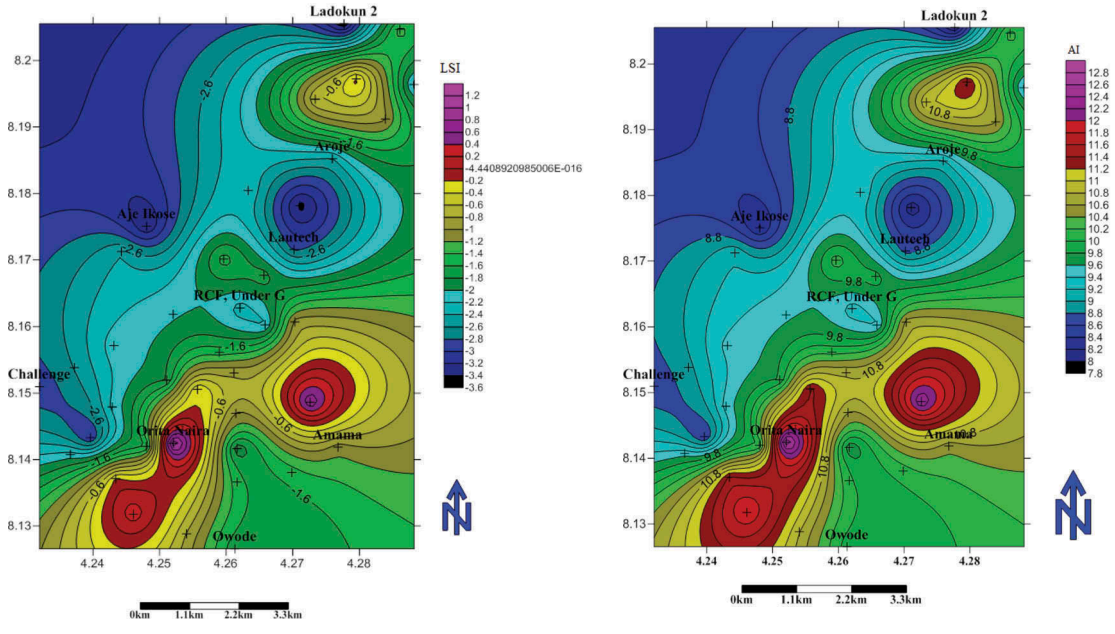

Figure 12. Corrosive index plot of groundwater in Ogbomoso North, southwestern Nigeria: (a) Langelier saturation index; (b) aggressive index.

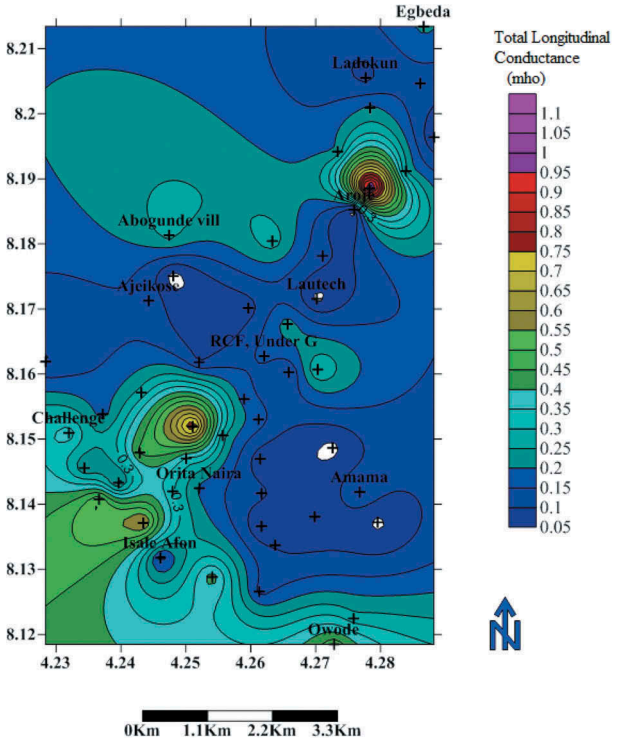

Figure 13. Total longitudinal conductance of the overburden.

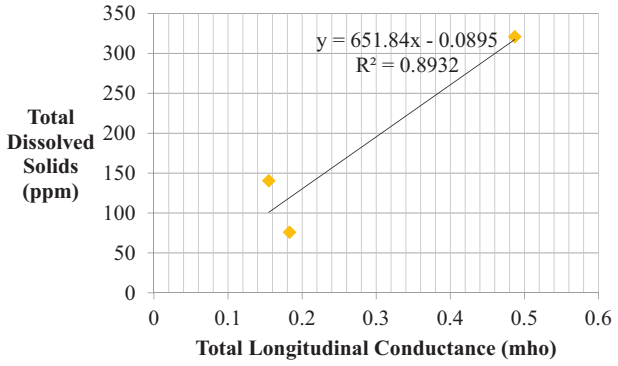

Figure 14. Total longitudinal conductance calibration curve based on median ranked TDS and median total longitudinal conductance.

4.7. Aquifer overburden protective capacity

The overburden protective capacity of the aquifers, determined by ranking the total longitudinal conductance in terms of the TDS based on classification in Figure 10(a) using Equation (12), is depicted in Table 4. It indicates the aquifer overburden protective capacity is poor, fair, good and excellent when the total longitudinal conductance exceeds 0.7657 mho, ranges within 0.4619–0.7657 mho, varies within 0.1535–0.4604 mho and is less than 0.1535 mho, respectively. In contrast, the overburden protective capacity rating using the TDS computed from Equation (12), employing the total longitudinal unit conductance as is standard in most literature (e.g. Oladapo et al. 2004; Ayolabi 2005; Oladapo and Akintorinwa 2007; Atakpo and Ayolabi 2009; Obiora et al. 2015; Bayewu et al. 2018), based on Henriet (1976), is given in Table 5. It indicates the overburden protective capacity ratings show fair agreement (moderate/Good–fair) at a total longitudinal conductance interval of 0.2–0.69 mho. This could be attributed to the fact that while the calibration equation for the total longitudinal conductance and hence overburden protective capacity rating was based on TDS values vis-à-vis the WHO (2011) acceptable values, the longitudinal unit conductance which in terms of aquifer protection gets a dimension of time; infiltration time (Henriet 1976) or vertical times-of-travel (Kalinski et al. 1993), which should be determined for unsaturated ground water protective layers. Furthermore, while the calibration in the current study was based on values for the parameters obtained in a typical crystalline basement environment, Henriet's (1976) application was for a set of carboniferous limestone basins but had been used in different geologic terrain, basement complex (e.g. Oladapo et al. 2004; Oladapo and Akintorinwa 2007; Obiora et al. 2015; Bayewu et al. 2018) and sedimentary environment (e.g. Ayolabi 2005; Atakpo and Ayolabi 2009). These suggest overburden protective capacity rating is site specific – that is, dependent on the local geology and the prevailing anthropogenic influences – and should be determined as such.

Table 4. Overburden protective capacity rating for crystalline basement groundwater in Ogbomoso North, southwestern Nigeria.

TDS (ppm)	Total longitudinal conductance (mho)	Overburden protective capacity rating
<100	<0.1535	Excellent
100–300	0.1535–0.4604	Good
301–499	0.4619–0.7657	Fair
>500	0.7672 and above	Poor

Table 5. Overburden protective capacity rating based on Henriet 1976 vis-à-vis the current study.

Henriet (1976), Oladapo et al. (2004)		Current study	
Total longitudinal conductance (mho)	Overburden protective capacity rating	TDS*	Overburden protective capacity rating
>10	Excellent	7170	Poor
5–10	Very good	3259–6518.4	Poor
0.7–4.49	Good	456.2–2926.76	Poor
0.2–0.69	Moderate	130.28–449.68	Good–fair
0.1–0.19	Weak	65.09–123.76	Excellent–good
<0.1	Poor	<58.58	Excellent

* Based on regression equation (12) for calibration of total longitudinal conductance.

5. Conclusion

The overburden protective capacity and groundwater corrosion in the basement complex of Ogbomoso North, southwestern Nigeria, was determined. The overburden protective capacity assessment was based on calibration of the total longitudinal conductance S computed from iterative interpretation of vertical electrical soundings acquired near well bores using in situ measured total dissolved solids of the water samples from the well bore. The groundwater corrosion was determined using the Langelier saturation index and the aggressive index.

The total longitudinal conductance computed for the apparent resistivity curves which were predominantly H type and its admixture (namely KH, QH, HA and HKH types), ranged from 0.037995 mhos to 1.10878 mhos. The computed LSI and AI ranged from −3.61 to 1.20 and from 7.8 to 12.8, respectively. While high LSI (0.2–1.2) and AI (11.2–12.8) values in the southwestern part suggest the groundwater in this section of the study area is strongly corrosive, the low values of LSI (−3.6 to −1.2) and AI (7.8–10.2) in the northwest and southeastern parts indicate the groundwater there is non-corrosive. These findings suggest the groundwater corrosion in the study area is localised.

The regression equation obtained from the S-calibrated curve based on TDS indicates a strong positive correlation ($R^2 = 0.8932$). The calibrated curve revealed the overburden protective capacity ranged from excellent to good, fair and poor with corresponding S values of <0.1535 mho, 0.1535–0.4604 mho, 0.4619–0.7657 mho and ≥ 0.7672 mho, respectively, for the study area, based on equivalent TDS values vis-à-vis the WHO tolerance levels. However, the overburden protective capacity rating using Henriet total longitudinal conductance intervals indicated otherwise, based on TDS values using the calibrated equation obtained for the study area: it showed fair agreement (moderate/good–fair) at a total longitudinal conductance interval of 0.2–0.69 mho. These indicate that overburden protective capacity ratings are site specific, dependent on the local geology and the prevailing anthropogenic influences, which should be determined.

The corroboration of S and spatial distribution maps of TDS, LSI and AI suggest a groundwater corrosion index can be used as proxy for overburden protective capacity assessments.

Acknowledgements

The authors are grateful to the National Research Institute of Astronomy and Geophysics for generous support for the publication of this research article at no cost.

Disclosure statement

No potential conflict of interest was reported by the authors.

ORCID

M. A. Adabanija http://orcid.org/0000-0002-3737-0350

References

Adabanija MA 2009. Modification and application of genetic algorithm and simulated annealing to model estimation and appraisal in 1-D inversion of apparent resistivity data. PhD thesis, Department of Geology, University of Ibadan, Ibadan 265pp

Adabanija MA, Afolabi AO, Olatunbosun AT, Kolawole LL. 2015. Integrated approach to investigation of occurrence and quality of groundwater in Ogbomoso North, Southwestern Nigeria. Environ Earth Sci. 73(1):139–162. doi:10.1007/s12665-014-3401-8.

Adabanija MA, Omidiora EO, Olayinka AI. 2008. Fuzzy logic modeling of resistivity and hydrogeologic parameters for aquifer assessment in basement complex. Hydrogeol J. 16(3):461–481. doi:10.1007/s10040-007-0221-x.

Afolabi OA, Kolawole LL, Abimbola AF, Olatunji AS, Ajibade OM. 2013. Preliminary study of the geology and structural trends of lower proterozoic basement rocks in Ogbomoso, SW Nigeria. J Environ Earth Sci. 3 (8):82–95.

Akinwumiju AS, Olorunfemi MO. 2017. A GIS-based aquifer vulnerability assessment in the basement complex terrain of southwestern Nigeria. Sustain Water Resour Manag. 1–20. doi:10.1007/s40899-017-0157-9.

American Water Works Association. 1977. Standard for asbestos-cement distribution pipe, 4 in. through 16 in. for water and other liquids: AWWA C400-77. Denver (CO): American Water Works Association; p. 20.

Atakpo EA, Ayolabi EA. 2009. Evaluation of aquifer vulnerability and the protective capacity in some oil producing communities of Western Niger Delta. Environmentalist. 29:310–317. doi:10.1007/s10669-008-9191-3.

Ayolabi EA. 2005. Geoelectric evaluation of Olushosun landfill site Southwest Nigeria and its implication on groundwater. J Geol Soc India. 66:318–322.

Babiker LS, Mohamed AAM, Higama T, Kato K. 2005. A GIS-based DRASTIC model for assessing aquifer vulnerability in Kakami Gahar Heights, Gifu Perfecture, Central Japan. Sci Total Environ. 3(5):127–140.

Barker R, Rao TV, Thangarajan M. 2001. Delineation of contaminant zone through electrical imaging techniques. Curr Sci. 81(3):277–283.

Bayewu OO, Oloruntoba MO, Mosuro GO, Laniyan TA, Ariyo SO, Fatoba JO. 2018. Assessment of groundwater prospect and aquifer protective capacity using resistivity method in Olabisi Onabanjo University Ago Iwoye southwestern Nigeria. NRIAG J Astron Geophys. 15pp. doi:10.1016/j.nrjag.2018.05.002.

Belitz K, Jurgens BC, Johnson TD, 2016. Potential corrosivity of untreated groundwater in the United States. US Geological survey scientific investigations report 2016–5092, 16. doi 10.3133/sir20165092

Clifford J, Binley A. 2010. Geophysical characterisation of riverbed hydrostratigraphy using electrical resistance tomography. Near Surf Geophys. 8(6):493–501. Corrosionpedia.com/21-types-of-pipe-corrosion-failure/ accessed March 19, 2020

De Oliveira Braga AC, Filho WM, Dourado JC. 2006. Resistivity (DC) method applied to aquifer protection studies. Rev Bras Geofis. 24(4):573–581.

Deppermann K, Homilius J. 1965. Interpretation of geoelectrical sounding curves by investigating sub-surface groundwater. Geol Yearb. 83:563–573.
Dhakate R, Singh VS. 2005. Estimation of hydraulic parameters from surface geophysical methods, Kaliapam ultramafic complex, Orissa India. J Environ Hydrol. 13(12):1–11.
Edwards M, Triantafyllidou S. 2007. Chloride–to–sulfate mass ratio and lead leaching to water. J Am Water Works Assn. 99(7):96–109.
Golam SS, Keramat M, Shahid S. 2016. Deciphering transmissivity and hydraulic conductivity of the aquifer by vertical electrical sounding (VES) experiment in Northwest Bangladesh. Appl Water Sci. 6:35–45.
Henriet JP. 1976. Direct applications of the dar zarrouk parameters in ground water surveys. Geophys Prospect. 24:344–353. doi: 2 doi:10.1111/gpr.1976.24.issue-2.
Hodlur GK, Dhakate R, Andrade R. 2006. Correlation of vertical electrical sounding and borehole-log data for delineation of salt water and fresh water aquifers. Geophysics. 71:G11–G20
Hodlur GK, Dhakate R, Sirisha T, Panaskar DB. 2010. Resolution of freshwater and saline water aquifers by composite geophysical data analysis methods. Hydrol Sci J. 55(3):414–434. doi:10.1080/02626661003738217.
Hu J, Gan F, Triantafyllidous S, Nguyen CK, Edwards MA. 2012. Copper-induced metal release from lead pipe into drinking water. Corrosion. 68(11):1037–1048. doi:10.5006/0616.
Hwang SH, Shin JH, Park IH, Lee SK. 2004. Assessment of seawater intrusionusing geophysical well logging and electrical soundings in a coastal aquifer, Youngkwang-gun, Korea. Explor Geophys. 35:99–104.
Iliopoulus V, Stamatis G, Stournaras G. 2011. Marine and human activity effects on groundwater quality of Thriassio Plain. Attica (Greece). In: Lambrakis N, Stournaras G, Katsanou K (eds) Advances in the Research of Aquatic Environment. Environmental Earth Sciences. Springer, Berlin, Heidelberg doi:10.1007/978-3-642-24076-8_48.
Ismail A, Anderson NL, Rogers JD. 2005. Hydrogeophysical investigation at Luxor, Southern Egypt. J Environ Eng Geophys. 10(1):35–50.
Kalinski RJ, Kelly WE, Bogardi I, Pesti G. 1993. Electrical resistivity measurements to estimate travel times through unsaturated ground water protective layers. J appl geophys. 30(3):161-173. doi: 10.1016/0926-9851(93)90024-S.
Keswick BH, Wang D, Gerba CP. 1982. The use of microorganisms as groundwater tracers – A review. Groundwater. 20(2):142–149.
Khalil MH. 2006. Geoelectric sounding for delineating salt water intrusion in the Abu Aenima area, west Sinai, Egypt. J Geophys Eng. 3(3):243–251. doi:10.1088/1742-2132/3/3/006.
Kwang Y, Scho H, Jehyun S, Intwa P, Sang K. 2004. Assessment of seawater intrusion using geophysical well logging and electrical soundings in coastal aquifers. Explor Geophys. 35:99–104.
Langelier WF. 1936. The analytical control of anti-corrosion water treatment. J Am Water Works Assn. 28(10):1501–1521.
Langland MJ, Dugas DL, 1996. Assessment of severity and distribution of corrosive ground water in Pennsylvania. US Geological Survey Open-file Report 95–377
Larson TE, Buswell AM. 1942. Calcium carbonate saturation index and alkalinity interpretations. J Am Water Works Assn. 34(11):1667–1684.
Linderholm P, Marescot L, Loke MH, Renaud P. 2008. Cell culture imaging using microimpedance tomography. IEEE Trans Biomed Eng. 55(1):138–146.
Machiwal D, Cloutier V, Güler C, Kazakis N. 2018. A review of GIS-integrated statistical techniques for groundwater quality evaluation and protection. Environ Earth Sci. 77:681–687. doi:10.1007/s12665-018-7872-x).
Maillet R. 1947. The fundamental equations of electrical prospecting. Geophysics. 12:529–556. doi:10.1190/1.14373421070485X.
Mastrocicco M, Vignoli G, Colombani N, Zeid NA. 2010. Surface electrical resistivity tomography and hydrogeological characterization to constrain groundwater flow modeling in an agricultural field site near Ferrara (Italy). Environ Earth Sci. 61(2):311–322.
McFarland ML, Provin TL, Boellstorff DE. 2011. Drinking water problems: Corrosion. Texas AgriLife Extension Service, Department of Soil and Crop Sciences, Texas. SCS-2011-03, 6pp.
Millette JR, Hammonds AF, Pansing MF, Hansen EC, Clark PJ. 1980. Aggressive Water: assessing the Extent of the Problem. J Awwa. 72(5):262.
Mirribasi R, Mazloumzadeh SM, Rahnama MB. 2008. Evaluation of irrigation water quality using Fuzzy logic. Res J Environ Sci. 2(5):340–352.
Obiora DN, Ajala AE, Ibuot JC. 2015. Evaluation of aquifer protective capacity of aquifer unit and soil corrosivity in Makurdi, Benue State Nigeria using electrical resistivity method. J Earth Syst Sci. 124(1):125–135.
Oladapo MI, Akintorinwa OJ. 2007. Hydrogeophysical study of ogbese southwestern nigeria. Glob J Pure Appl Sci. 13(1):55-61. doi:10.4314/gjpas.v13i1.16669.
Oladapo MI, Mohammed MZ, Adeoye OO, Adesola OO. 2004. Geoelectric investigation of the Ondo State housing corporation Estate Ijapo Akure southwestern Nigeria. J Min Geol. 40(1):41–48.
Oladunjoye MA, Adabanija MA, Oni AA. 2013. Groundwater prospecting and exploration in a low potential Hard Rock Aquifer: case study from Ogbomoso North, South-western Nigeria. J Environ Earth Sci. 3(14):84–102.
Olasehinde PI. 2015. Statistical assessment of groundwater quality in Ogbomosho, Southwest Nigeria. Am J Min Metall. 3(1):21–28. doi:10.12691/ajmm-3-1-4.
Pieper KJ, Krometis LAH, Gallagher DL, Benham BL, Edwards M. 2015. Incidence of water borne lead in private drinking water systems in Virginia. J Water Health. 13(3):897–908. doi:10.2166/wh.2012.275.
Rahaman MA. 1976. Review of the basement geology of Southwestern Nigeria. In: Kogbe CA, editor. Geology of Nigeria. Lagos: Elizabethan Pub. Co; p. 41–58.
Rasolofonirina M, Randriamanivo LV, Andrianarilala MT, Andriambololona R, 2004. Trace Elements and Physicochemical quality of the well waters in Mahitsy, Province of Antananarivo, Madagascar. HEPMAD'04 international conference; September 27–October 1; Madagascar.
Roberge PR. 2007. Corrosion inspection and monitoring. John Wiley & Sons: New York; p. 4. appendix B. doi:10.1002/9780470099766.app2.
Rupert MG. 2001. Calibration of the DRASTIC groundwater vulnerability mapping method. Ground Water. 39:630–635.
Schock MR, Buelow RW. 1981. The behaviour of asbestos-cement pipe under various water quality conditions: part 2, Theoretical considerations. J Am Water Works Assn. 73(11):609.

Singley JE, Beaudet BA, Markey PH, DeBerry DW, Kidwell JR, Malish DA. 1985. Corrosion prevention and control in water treatment and supply systems: park Ridge. New Jersey: Noyes Publications.

Storz H, Storz W, Jacobs F. 2000. Electrical resistivity tomography to investigate geological structures of the Earth's upper crust. Geophys Prospect. 48(3):455–471.

WHO. 2011. Guidelines for drinking-water quality. 4th ed. Geneva: World Health Organization.

Zhu GF, Su YH, Feng Q. 2008. The hydrochemical characteristics and evolution of groundwater and surface water in the Heihe River Basin, northwest China. J Hydrol. 16:167–182.

Zohdy AAR, Eaton GP, Mabey DR, 1974. Application of surface Geophysics to ground-water investigations. Technique of water resource investigation series Book 2, Section DI Washington Department of the Interior USGS 116pp

Zuquette LV, Failache M. 2018. Mapping groundwater pollution vulnerability with application in a basin southern Brazil. Environ Earth Sci. 77:689. doi:10.1007/s12665-018-7862-z.